VORTEX FLOW VISUALIZATIONS INSIDE AND AFTER THE SURFACE DIMPLES OF DIFFERENT SHAPE AND CONFIGURATION

A.A. KHALATOV [1], V.I. TEREKHOV [2]

[1] Institute of Engineering Thermophysics, National Academy of Science, Kiev, 03057, Ukraine
[2] Institute of Thermophysics, Russian Academy of Sciences, Siberian Branch, Novosibirsk, 630090, Russia

Corresponding author (1): Tel.: +38 044 456-9302; Fax: +38 044 456-6091; E-mail: Artem.Khalatov@vortex.org.ua

INTRODUCTION

Over the last twenty years the intensive research effort was focused on studies of hydrodynamics and heat transfer over surfaces with indentations (dimples). The early discoveries of low drag penalties for golf balls were made in [1] demonstrating the effectiveness of the shallow surface dimples to cause the pressure losses and early boundary layer transition without the drag penalties associated with sand roughness. Unlike round balls with either smooth or sand roughened surfaces, the dimpled ball drag curve remains almost constant at the supercritical Reynolds numbers (Fig.1). Due to reductions in the backside separation zone the drag coefficient of a dimpled ball at Re<60,000 is substantially lower than that over a sanded or smooth ball. These results indicate the dimples have a more beneficial effect on the drag reduction and laminar-turbulent transition than sand roughness.
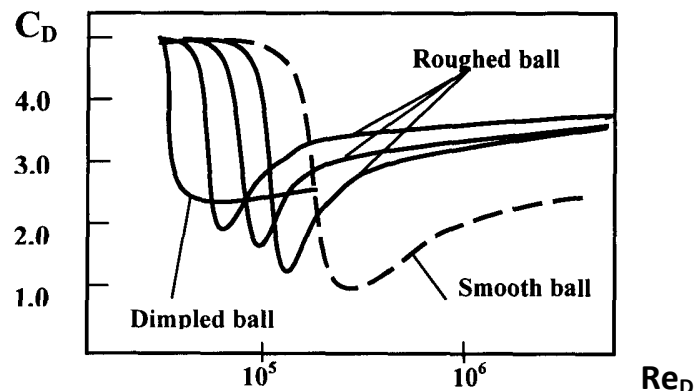
Figure 1. Drug coefficient of smooth, roughed and dimpled balls [1].

These important issues resonated in a few international research programs. Even initial studies focusing on a single spherical dimple on a flat plate have shown the fundamental potential of this technique for heat transfer augmentation as they produce substantial heat transfer augmentation rates with pressure drop factors, which are smaller than other types of heat transfer augmenters. The Russian researchers were the first who revealed the in-dimple «side-to-side» fluctuating vortex at relatively higher Reynolds numbers [2]. The further precise flow visualizations have disclosed the «tornado-like» nature of this vortex with substantial in-vortex energy concentration.

In terms of the in-dimple flow pattern, the spherically shaped dimples as studied in more detail can be classified, as [3]: (i) shallow dimples (h/D ≤ 0.10), (ii) deep dimples (h/D>0.20), (iii) intermediate depth dimples (h/D=0.10…0.20). There is no separation zone inside shallow dimples, generating the Görtler vortices over a concave dimple surface and the Karman «vortex street» after a dimple. Likewise, no side-to-side fluctuating vortex was found in dimples with h/D < 0.13. For the intermediate and deep dimples the Karman vortex street appears at Re_D= 600…800 and transforms into the twin vortex structures between $Re_D ≈$ 1,000 and 3,200. In

dimples with h/D > 0.15 the weak side-to-side fluctuating vortex appears at $Re_D \approx 4,000$ and transforms into the stable fluctuating vortex structures by $Re_D \approx 5,500$. In an intermediate dimple (h/D = 0.13) the twin vortex may exist up to $Re_D = 100,000$. These conclusions have been made for the spherical dimple with sharp-edged border; however no fluctuating vortex was found in a deep spherical dimple (h/D = 0.26) with rounded-off border, as well as in a deep dimple (h/D=0.50) up to Re_D= 350,000 at the supersonic flow (M = 4.0) [6].

Despite the substantial available database many important vortex flow features was not disclosed so far, therefore the extensive research program was undertaken in the Ukrainian Academy of Sciences over twenty years ago to investigate some precise flow features in the shallow spherical and cylindrical dimples (h/D≤010) on a flat plate arranged in various configurations. The experimental part of this program was established in the Aeronautic Lab of the U.S. Air Force Academy (Colorado Springs, CO) using the unique water tunnel, visualization technique and measurement systems.

TEST FACILITY AND VISUALIZATION TECHNIQUE

The experimental program was performed in a closed-circuit water tunnel (Fig. 2) capable of operating over a speed range of 0.05 m/s to 0.50 m/s [3, 5]. An axial flow pump is capable of producing a volumetric flow rate of 0,7 m^3/s. The test channel is 1,830 mm long with the rectangular cross section (610 mm height x 457 mm width). The side walls and floor are made from a glass to allow flow structure observations. The inlet nozzle has a contraction of 6 : 1, the inlet turbulence intensity is less than 1.0%. The mean velocity angularity is around ± 1.0 degrees in both pitch and yaw directions. The test section (Fig. 3) is an acrylic flat plate (19 mm thick) into which various dimple configurations might be machined. The flat plate has an elliptic leading edge, it is 1,220 mm long and 381 mm width.
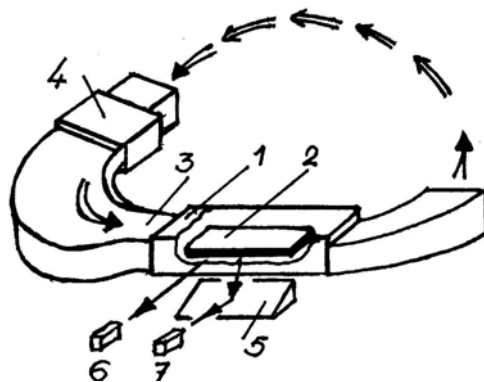
Figure 2. Schematic view of the U.S. Air Force Academy water tunnel [3]. 1 -test channel. 2 -test section. 3 -inlet nozzle. 4 - axial flow pump. 5 - inclined floor mirror. 6 - digital camcorder: side observations. 7 – digital camcorder: top observations.
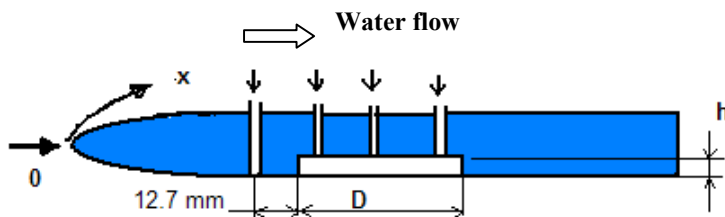
Figure 3. Test section with elliptic leading edge.

To visualize flow vortex structures, five different colors of dye were injected through five cylindrical ports machined both upstream and inside of a representative dimple (Fig. 3). The dimpled flat plate was suspended down in the water tunnel, so the flow structures could be observed through the transparent floor with the aid of an inclined mirror placed below the water tunnel test section. A digital camcorder (SONY-DCR VX2000) was used to record the flow patterns within and downstream of the dimple(s). A second camcorder was installed facing one of the side walls, so that observations could be made from a side view perspective. All video

images were stored as digital (AVI) files to allow computer screening at a reduced frame rate with Adobe Premiere 6.5 Software. In this way, the flow structures and patterns could be carefully observed, analyzed and characterized. Two-Dimensional Laser Doppler Velocimeter (LDV) System was also employed to measure velocity profiles in-front and downstream of dimple(s).

The uncertainty of Reynolds was estimated to be within $\pm 2.4\%$, velocity measurements were calibrated within 1.8%. The uncertainty in frequency of bulk flow oscillations was estimated to be $\pm 10.6\%$ which contributed to an uncertainty in the Strouhal number of $\pm 10.9\%$. Measurements of the extent of the separation zone inside the dimple are estimated to be within $\pm 7.8\%$ of the dimple diameter. All uncertainty estimates are based on the methods of Coleman and Steele [4].

SINGLE DIMPLE

All dimples have identical surface diameter D of 50.8 mm (Fig. 2). The test cases involving three different dimple configurations are given in the Table. All dimples were machined at a distance of 88 mm from the test section leading edge to the dimple center. In experiments Reynolds number Re_D range was from 3,100 to 23,590. This corresponds to a range of Reynolds number Re_x based on the axial distance from the leading edge to the dimple leading rim of 3,820 to 29,060. The ratio of pre-dimple relative boundary layer thickness in-front of the dimple (δ_{00}/h) was 0.25…0.30 across the entire range of Reynolds number. As the LDV flow measurements have shown at these flow conditions the flow in-front of a dimple was the laminar one for all configurations tested.

Table. Dimple test cases and geometric parameters

No	Dimple case	h , mm	h/D
1.	Single spherical dimple	5.08	0.10
2.	Single cylindrical dimple	5.08	0.10
3.	Single cylindrical dimple	2.54	0.05

Spherical dimple

At low speeds (Re_D=3,300…4,200) all streamlines over the single dimple were quite parallel and only small fluctuations of 1…2 Hz were observed along the center streamline (labeled C-streamline in Fig.4.a). These fluctuations were confined to a small zone near the downstream edge of the dimple. As Re_D was increased to 5,100 , a separation zone arises inside the dimple along the downstream edge of the dimple. The size of this separated region grew constantly as Re_D increased to 23,450. The most appreciable growth in the size of the separated zone occurred in Re_D range of 5,100 to 6,700. As Re_D was increased above 4,200 the C-streamline fluctuations continued to increase in the frequency. Figure 4.b shows that both off-center streamlines (labeled S1-streamlines) became involved in the Karman vortex street type fluctuations starting at Re_D=6,700. Also, the streamlines aligned with the dimple edges (labeled S2-streamlines) demonstrated a slight deviation toward the dimple edges due to an apparent suction effect.

As Re_D was increased above 6,700, there was a slow and periodically alternating clockwise and counter-clockwise bulk flow rotation inside the dimple with an accompanying periodic migration of the separation zone between the dimple centerline and the upper S2-streamline as shown in Fig. 4.c. These rotational fluctuations ceased at Re_D= 12,200, at which point the separation zone became symmetrical with respect to the dimple centerline as shown in Fig. 4.d. At Re_D= 7,900 , a weak twin vortex appeared inside the non-separated zone of the dimple. The «strength» of this vortex grew as Re_D increased while both S2-streamlines were drawn inwards toward the dimple. Thus between Re_D= 12,200 and Re_D= 21,000 , the flow inside the dimple included both a twin vortex and a region of flow separation. The curved upstream edge of the separated region appears to discharge pulses of mass flow into the separation zone. This appears to be the source of the bulk flow fluctuations. Figure 4.d shows that although the wake region downstream of the dimple is wider than that of a dimple surface border, the source of the fluctuations is only approximately 0.75·D in
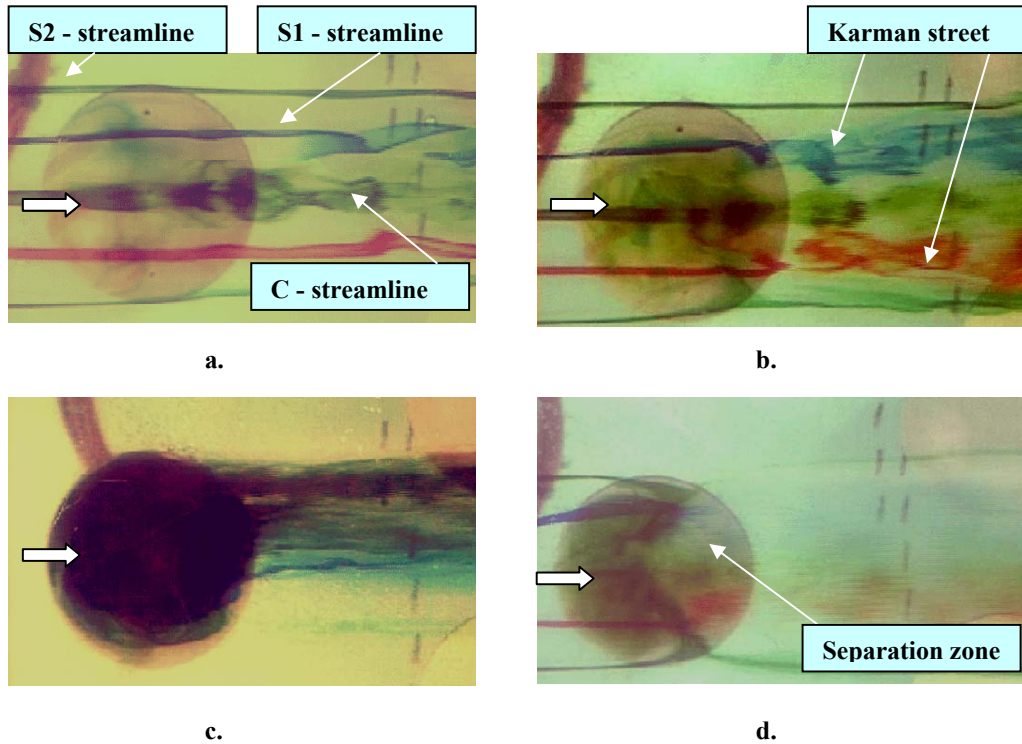
Figure 4. Spherical dimple (dye injection from inside ports).

a: Re_D= 4,200. **b:** Re_D= 6,700. **c:** Re_D= 9,300. **d:** Re_D= 17,900.

a width. Finally, as Re_D was increased to 23,450, the separation zone inside the dimple becomes very large which led to the elimination of the twin vortex structure. Only the chaotic streamlines could be seen within the non-separated zone near the upstream edge of the dimple. The maximum frequency of bulk flow fluctuations ($f \approx 13Hz$) was found at Re_D=17,900, when both S2-streamlines were fully drawn into the dimple as shown in Fig. 4.d.

Cylindrical dimple (h/D=0.10)

Before the basic experimental program, LDV measurements were performed in front of the cylindrical dimple ($x = x_D$) to identify the pre-dimple flow parameters [3]. The flow fields were scanned upstream of the dimple front edge both on the dimple centerline and in the span-wise direction $0.25 \cdot D$ and $0.5 \cdot D$ off the centerline. Comparisons with the Blasius solution revealed differences between measured and predicted values occurred to be within +/- 10%. As concluded, it is due to effect of the elliptical leading edge generating the local gradient flow.

At $x_D/D = 0,66$ upstream of the dimple and over the centerline (Fig. 5.a) the axial velocity profile corresponds to the shear flow, however small reductions in the velocity profile can be seen above the boundary layer edge. Apparently, it is due to the convex curvature effect of the leading edge area. At the same upstream location, but $z = \pm 0,25 \cdot D$ off the centerline in the span-wise direction (Fig. 5.b), the effect of the in-dimple flow separation zone, unsteadiness, is present and the velocity profile experiences significant fluctuations in the normal direction. The average velocity profile, presented in Fig. 5.b shows the «distortion zone» thickness is $\approx 1\,0$ mm ($y/h \approx 0,20$). Further from the dimple centerline ($z = \pm 0,5 \cdot D$), the velocity profile is close to the shear flow shape as given in Fig. 5.a.

The flow that reaches the edge of a cylindrical dimple sees a more abrupt drop off than for the flow approaching a spherical hole. For the flow along the dimple centerline, it is much more like flow over a backward facing step. At the lowest velocity (Re_D= 3,200) the fluctuations of the C-streamline and S1-streamlines were of the Karman type and were clearly seen. They were accompanied with periodic bulk flow oscillations along the dimple axis. It is the laminar flow zone both in-front and after a dimple. At

$Re_D > 4,000$ the fluctuations of the S1-streamlines continued to grow along with more vigorous bulk flow oscillations at the dimple axis. The zone of separated flow at the C- and S1-locations formed at $Re_D = 3,200$ and grew rapidly up to $Re_D = 8,000$, where the length of the separation zone is $0.45 \cdot D$. As found from the direct flow field measurements, after cylindrical dimple ($h/D = 0.10$) the transition to turbulent flow happens after $Re_D \approx 6,500$. The counter rotating, convergent secondary flow formed along the downstream edge of the dimple at $Re_D = 4,100$ to transform into the weak twin vortex at $Re_D = 5,100$ as shown in Fig. 6.a. This twin vortex rotates slowly and continues to grow until $Re_D = 9,300$, where the maximum fluctuations were found. At $Re_D = 9,300$ the length of the separation zone was still $0.45 \cdot D$ being identical at both the centerline and at the $0.25 \cdot D$ offset (S1-location). For $Re_D > 6,600$ both S2-streamlines were drawn into the dimple space.
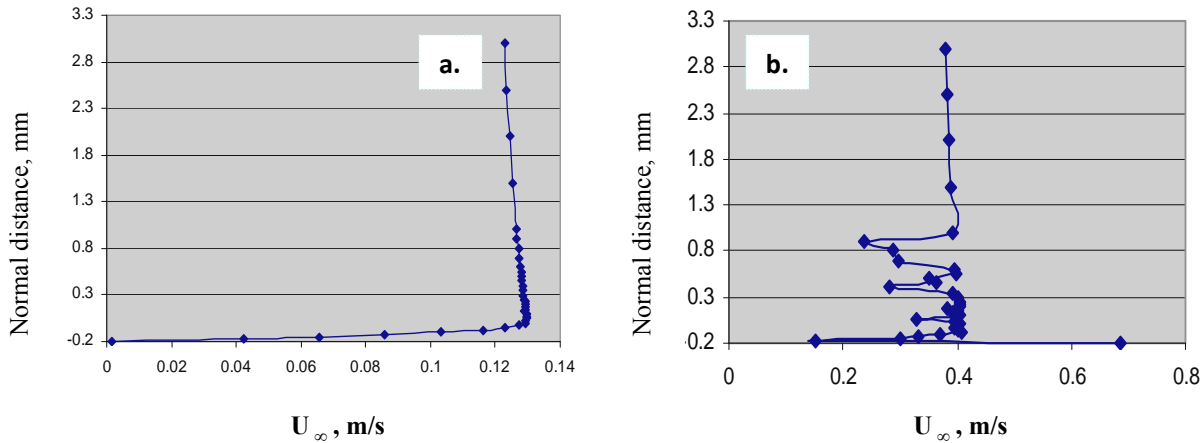
Figure 5. Average velocity profile upstream the cylindrical dimple ($x/D = 1,23$).

a: Dimple centerline. $U_\infty = 0,115$ m/s, $Re_D = 5,200$.   **b:** $0.25 \cdot D$ spanwise offset. $U_\infty = 0,36$ m/s, $Re_D = 16,200$.
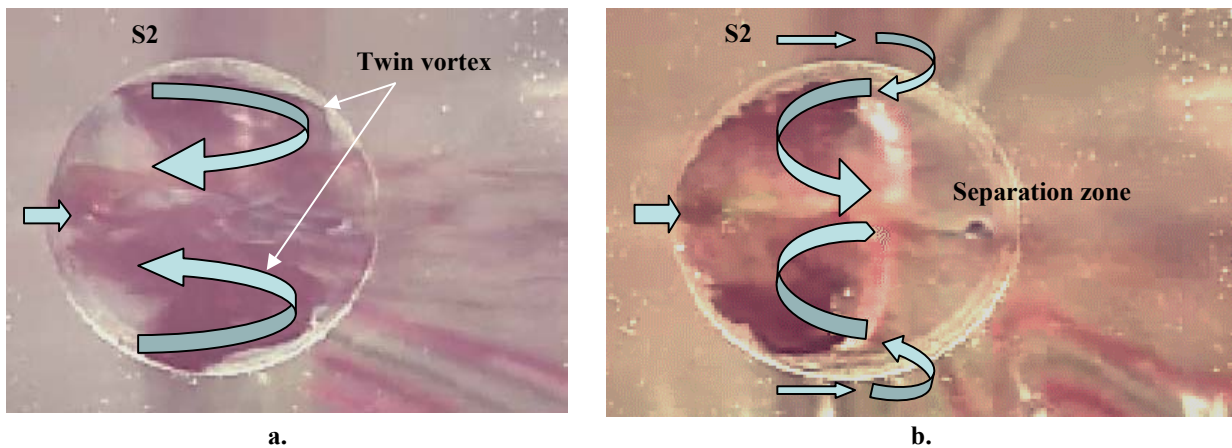
Figure 6. Cylindrical dimple, $h/D = 0.10$ (dye injection from inside ports). **a:** $Re_D = 8,000$. **b:** $Re_D = 12,250$.

For $Re_D > 9,300$, the S2-streamlines began to be drawn inwards towards the dimple projection. As Re_D was increased still further, they were drawn more and more into the dimple until they were fully captured at $Re_D = 15,000$. This is the Reynolds number «boundary» between two different in-dimple flow patterns. Two the S2- streamlines entering at $\pm 90^0$ are the origins of two counter rotating flows, moving toward the dimple leading edge. As a result, the legs of the twin vortex changed the sign of their rotation and

created a new vortex configuration with diverging flow at the separation line as shown in Fig. 6.b. It appears that this vortex configuration provides a more favorable condition for discharging the mass flow into the separation zone. The rate of the twin vortex rotation increased with Reynolds number, the extent of the separation zone grew to 0.73·D at Re_D= 23,450.

In-dimple separation zone

The length of the separation zone inside dimples was measured in two different locations, along the C-streamline and along the S1-streamlines (offset from the centerline by 0.25·D). Each length was measured as the distance between the beginning of the separated region and the downstream edge of the dimple. The data taken from the video images was processed and presented in Fig. 7 and Fig. 8 as the non-dimensional length (L/D) of the separated region plotted versus Reynolds number Re_D.
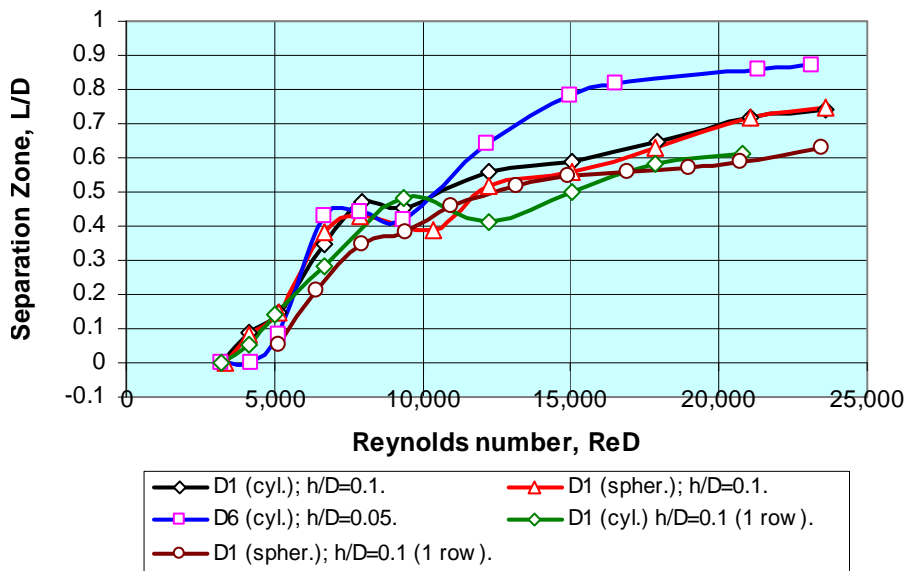
Figure 7. In-dimple separation zone depth (C-location): various dimple configurations.
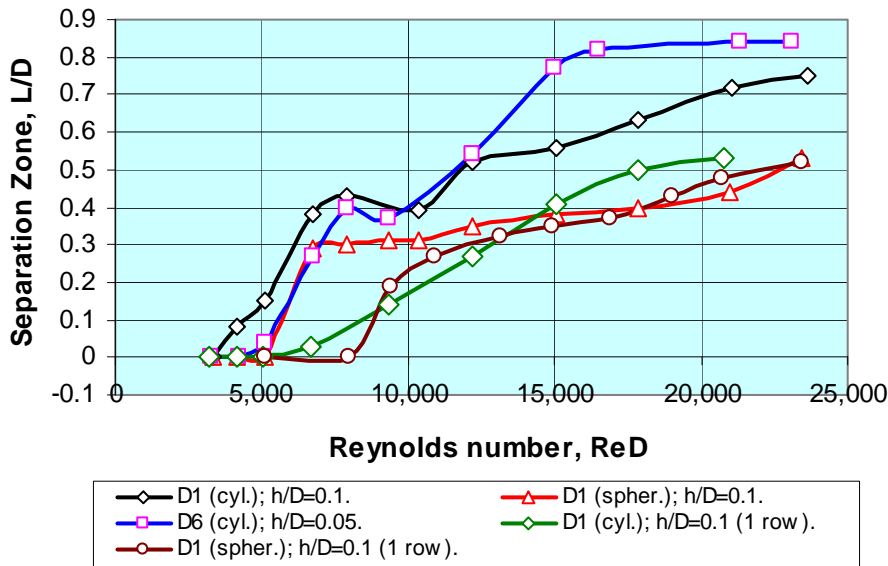
Figure 8. In-dimple separation zone depth (S1-locations): various dimple configurations.

Figure 8 presents the length of the separation zone over S1-streamline. This length increased rapidly with Re_D growth for all dimples. Again, at very high Reynolds numbers ($Re_D > 12,000$), the shallower cylindrical dimple has the largest separation zone length. Figure 7 indicates that at $Re_D < 12,000$, the length of separation zone is about the same as for the deeper cylindrical dimple. However at $Re_D > 12,000$ for S1-line the size of separation zone for the shallower cylindrical dimple exceeds that for all other dimple configurations (Fig. 8).

Bulk flow fluctuations

Preliminary experiments were performed on the single spherical dimple to identify suitable locations for the video camcorder to be placed along with locations for injecting the dye so that the bulk flow oscillations could be clearly observed and recorded. The experimental data taken from three different test set-ups yielded about the same value of Strouhal number across a wide range of Reynolds numbers. All three positions were used in subsequent measurements as a check for consistency.

Figure 9 is a plot of local Strouhal number versus Reynolds number Re_D, based on the dimple diameter. For all of the cases the Strouhal number curve has a maximum value at a certain Reynolds number and then drops off at higher Re_D. For the cylindrical dimples, the values of Sh_{max} are quite close each other. The Reynolds number corresponding to Sh_{max} for the spherical dimple is around two times greater than that for cylindrical dimples. Both at the low Reynolds numbers ($Re_D < 8,000$) and at the high Reynolds numbers ($Re_D > 12,000$), the Strouhal numbers for the spherical dimple are higher than those for the cylindrical dimples.
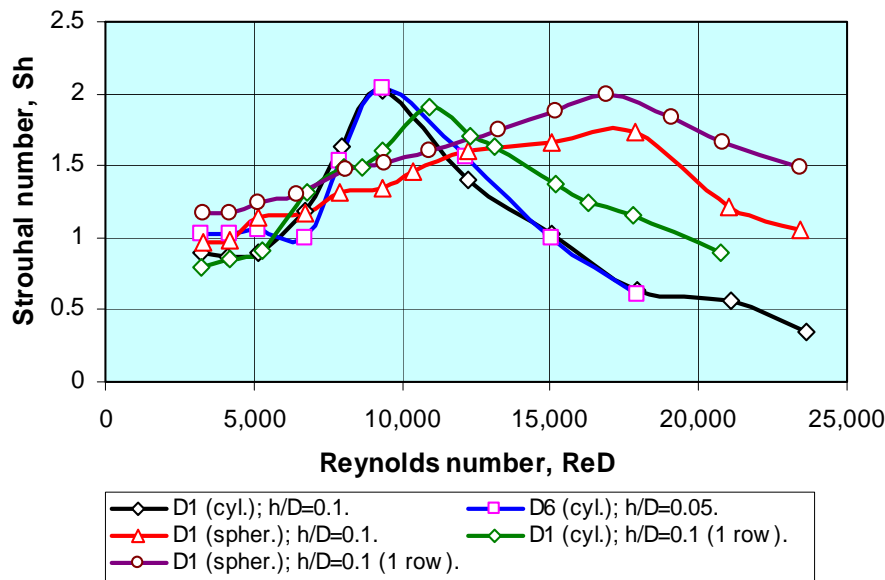
Figure 9. Bulk flow fluctuations (various dimple configurations).

As follows (Fig. 9), the vigorous growth in Strouhal number rate for the cylindrical dimple ($h/D=0.10$) begins at $Re_D > 6,000$. Therefore, the increase in the bulk flow fluctuations happens slightly earlier than the transition to the turbulent flow transition happens ($Re_D \approx 6,580$). However, this conclusion is valid for the range of dimple parameters studied and the δ_{00}/h ratio of $0.25…0.30$.

Effect of pre-dimple boundary layer thickness

To study effect of the pre-dimple boundary layer thickness both single cylindrical and spherical dimples were placed at the distance of $x/D=4,70$ (dimple center) from the test section leading edge. Unlike $x/D=1,23$ case, in the case of $x/D=4,70$ the ratio δ_{00}/h was varied from $0,88$ ($Re_D=16,240$) to $1,18$ ($Re_D=5,200$).

Cylindrical dimple. Increase in the boundary layer thickness greatly influences the flow pattern inside and downstream of a dimple. Starting at $Re_D=3,200$ the flow structure becomes unsteady and alternates. The small size and weakly fluctuating separation

bubble was formed behind the downstream dimple rim transforming periodically into the wide wake flow pattern downstream of the dimple. At Re_D>8,000 the flow continued to alternate however it demonstrated an asymmetric wake pattern. Starting at Re_D = 12,200 the separated flow forming inside the dimple accompanied the symmetrical wake downstream of the dimple. The separation zone grows monotonically up to Re_D =23,500, where the separation zone extent is around 0.45·D (Fig. 10.a). This is however 70% smaller than that for the dimple at x/D=1.23 and the same Re_D number. Inside the non-separated zone the flow streamlines are very irregular. Starting at Re_D = 18,000 the weak twin vortex type flow forms inside the dimple and grows slowly up to Re_D =23,500.

The periodic and stable bulk flow fluctuations downstream of the dimple began at Re_D > 10,000 (Fig. 11.a). These fluctuations are considerably lower than that observed for the cylindrical dimple at x/D=1.23. At Re_D> 16,500 the bulk fluctuations for both locations (x/D=1.23 and x/D=4.70) are actually the same which indicates that the pre-dimple boundary layer thickness had little effect.
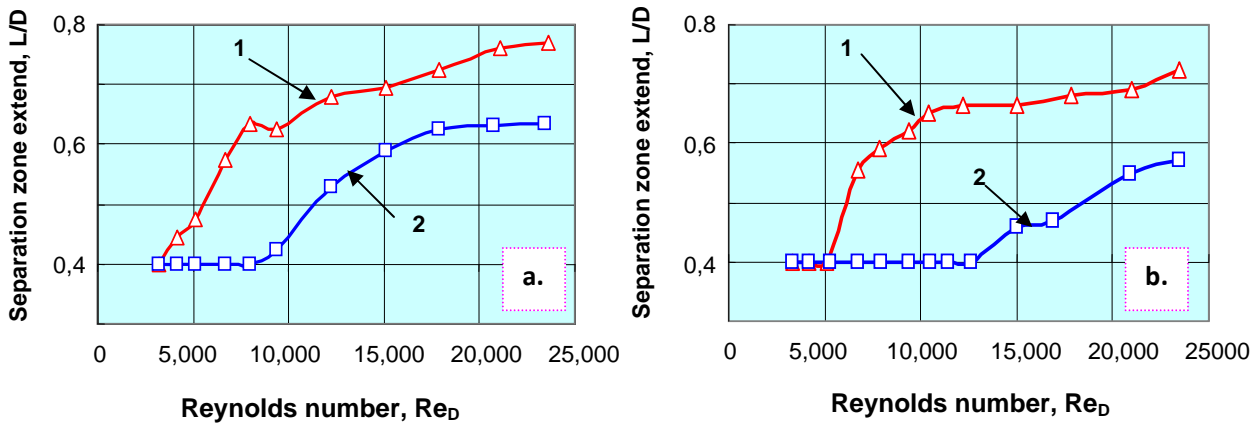
Figure 10. Extent of in-dimple separation zone over the centerline: cylindrical (a) and spherical (b) dimple.
1 – x/D = 1.23. **2** – x/D = 4.70.
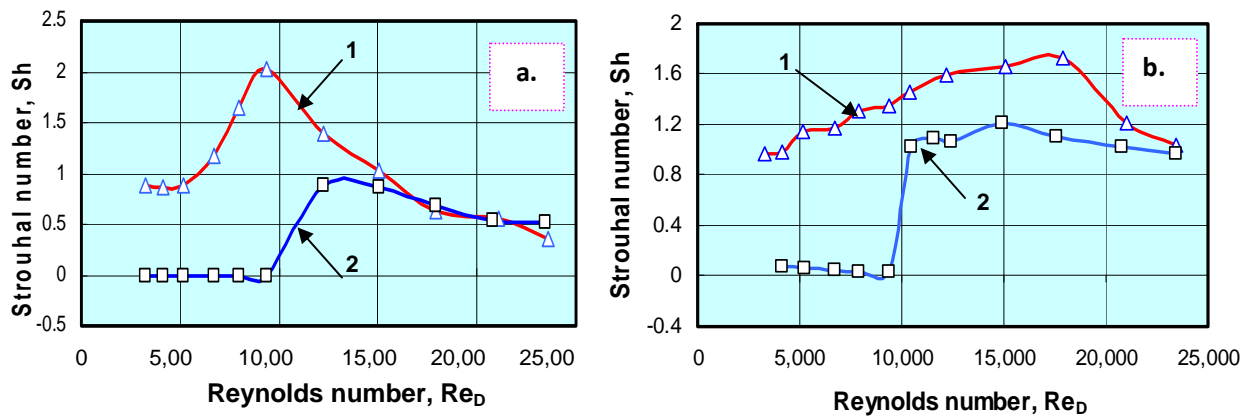
Figure 11. Bulk flow oscillations after cylindrical (a) and spherical (b) dimple. **1** – x/D = 1.23. **2** – x/D = 4.70.

Spherical dimple. At low velocities and up to Re_D=10,500 the flow downstream of the dimple was of the «strip type» transforming into asymmetrical wake flow at Re_D =11,400. An asymmetrical wake with a small separation bubble existed until Re_D=16,900, e.g. much longer than for the single spherical dimple located at x/D=1.23. The fully developed symmetrical flow after the dimple formed only after Re_D >17,000. However, the length of the in-dimple separation zone was much smaller than for the dimple located at x/D=1.23 (Fig. 10.b). The maximum separation zone length was 0.35·D, which was roughly half the size of the zone for the dimple at x/D=1.23.

The bulk flow fluctuations downstream of the spherical dimple became visible and regular only above $Re_D \approx 9,000$ (Fig. 11.b). Above this point the flow fluctuations grew very rapidly and reached the maximum Strouhal number at $Re_D \approx 15,000$. This occurred while there were the asymmetrical structures downstream of the dimple. As a whole, in the Reynolds number range of 10,000 to 17,000, the Strouhal number is of 40% to 50% lower of that for the dimple located at x/D =1.23. Over $Re_D \approx 24,000$, there is no effect of the boundary layer thickness on the downstream bulk flow fluctuations and the Strouhal numbers are virtually identical for both spherical dimples located at x/D=1.23 and x/D=4.7 at this elevated Re_D.

SINGLE ARRAY OF DIMPLES (x/D=1.23)

Cylindrical Dimples (h/D=0.10). Four additional dimples were machined alongside the existing cylindrical dimple to create a single array of dimples aligned in the span-wise direction. The primary feature of this configuration is a spanwise irregularity in the velocity due to the cross talk between the dimples. The representative dimple under the observation was in the middle with two identical dimples on either side.

Very small fluctuations of S1-streamlines (like shown in Fig. 4) occurred at Re_D=3,200 with a shallow separation zone at the dimple axis. The S2-streamlines were drawn into the dimple starting at Re_D=4,200 leading to the twin vortex formation. This twin vortex was fairly weak and disappeared completely by Re_D=10,900 , the point where the Strouhal number reached a maximum value. At low Reynolds numbers, the frequency of the bulk flow oscillations were close to that for a single dimple as shown in Fig. 9 although between Re_D=8,000 and Re_D=10,400, the Strouhal number dropped below that for a single dimple. At Re_D >10,400 the frequency of the dimple in a single array exceeded the single dimple frequency by up to 65%. Therefore dimples placed adjacent to one another do have an effect on each other.

Finally, adjacent dimples strongly influenced the shape of the separation zone making it narrower when compared with the single cylindrical dimple case. Figure 6 indicates that the length of the separation zone along the centerline remains about the same, however two S1 streamlines (offset from the center by 0.25·D) become shorter for the dimples in a single array.

Spherical dimples. At the low velocity (Re_D=3,200), transient vortex structures were observed in the form of twin vortices periodically forming and then destroying over the dimple space. The sequence of events has been registered and analyzed. At the beginning of the sequence, the S1-streamlines begin to twist and create a twin planar vortex that eventually affect the S2-streamlines. The random collision of either one of the twin vortex legs against the oscillating C-streamline results in the destruction of the twin vortex. This chaotic structure is then pushed out of the dimple in the downstream direction. After this, the flow returns to the parallel-streamline flow structure to begin the next repetitive sequence. This sequence repeated itself every 6…7 seconds.

For Re_D>3,200 , the flow structures were very similar to the single dimple case, although the onset of the various flow patterns appear to occur at lower values of Re_D. The weak fluctuations of the C-streamline (Karman street type) with gradually reduced side-to-side flow alternations were observed between Re_D = 3,300 and Re_D = 4,300. For Re_D > 4,300 , the separated region began to form along the downstream dimple edge. The alternation of weakly rotating flow in the clockwise, then counter-clockwise direction occurred in the range of Re_D between 5,100 and 6,400 which was much lower than that for the single dimple case (Re_D= 6,700 …12,200). At Re_D> 6,400, both S2-streamlines began to fluctuate and the flow pattern becomes symmetrical about the dimple centerline. Again, this event is similar to that shown for the single dimple case, but it occurred at a much lower value of Reynolds number.

The width of fluctuating flow existing downstream of the dimples in a row grew from 0.50·D at Re_D=9,400 to 0.82·D at Re_D=20,700. The twin vortex inside the dimple that began to form at Re_D=6,400, was destroyed by the time the Re_D had increased to 23,450. Although that was close to single dimple result, the rate of the twin vortex rotation was much greater than that for a single dimple.

Figure 7 shows the length of the separation zone along the centerline of the dimple, the C-streamline. The length of the separation zone for all dimple configurations of the same depth are about the same across the range of Re_D. However, at Re_D> 10,000, the shallow cylindrical dimple (h/D = 0.05) had a much longer separation zone than all other dimple configurations with h/D = 0.10. The greatest growth of the separation zone length occurs between Re_D= 5,000 and Re_D= 8,000, while between Re_D= 8,000 and Re_D= 10,000 the separation zone did not grow by any measurable amount. Figure 8 shows the length of the separation line along the S1-streamline, which is offset from the centerline by 0.25D. This length increased rapidly with Re_D for all of the single dimple configurations. At very high Re_D, the single cylindrical dimples have the largest separation zone length.

Figure 9 is a plot of local Strouhal number versus Reynolds number based on the dimple diameter. For all of the cases the Strouhal number curve reaches a maximum value at a critical Reynolds number and then drops off at higher Re_D. For all of the

cylindrical configurations, the values of Sh_{max} are quite close each other although it occurred for the dimples in array at a slightly higher Re_D. The Reynolds number corresponding to Sh_{max} for the spherical configurations is around two times greater than that for cylindrical configurations. Both at the low Re_D numbers ($Re_D<8,000$) and at the very high Reynolds numbers ($Re_D > 13,000$), the Strouhal numbers for the spherical dimple configurations were slightly higher than those for the cylindrical dimples.

DUAL ARRAY OF DIMPLES (x/D=1.23)

The experimental program was aimed to visualize details of the unsteady flow structure in front of, within and downstream of a dual array of shallow (h/D=0.10) spherical and cylindrical dimples placed on a flat plate. The center of the first array was located at 88 mm downstream of the elliptically-shaped leading edge of the plate (x/D=1,23) , the spanwise dimple pitch is 76.2 mm (S_z/D=1.50). The second array was arranged in a staggered mode with the same span-wise pitch and the downstream pitch between rows of 88 mm (S_x/D=1.73). The laminar flow existed in front of the first dimple array for all flow conditions studied. In front of the second array the flow structure appeared to have either laminar or turbulent flow depending on the Reynolds number and streamline location.

Cylindrical dimples. The experimental runs were conducted across the range of the water velocities from 0.072 to 0.52 m/s corresponding with diameter-based Reynolds numbers Re_D ranging from 3,260 to 23,450. The non-dimensional boundary layer thickness δ_{00}/h in front of the first array was 0.40 at $Re_D = 5,220$ and 0.28 – at $Re_D = 16,240$. Five different dye colors were injected through five cylindrical ports machined both upstream and inside the representative dimple.

The central streamline in the space between the first row adjacent dimples revealed a laminar flow structure in front of the second array dimple in the whole range of Reynolds number (up to $Re_D = 23,450$). At $Re_D \leq 4,200$ both S2 - streamlines were almost parallel to each other, while S3 - streamlines located in the wake of the first array experienced weak fluctuations. Fluctuations of S2 - streamlines observed only at $Re_D > 5,000$, with the laminar-turbulent flow transition (streamline destruction) completed by $Re_D \approx 12,250$. On both S3 - streamlines the turbulent structure indicated at $Re_D = 5,300$.

Inside a dimple, the flow began to separate at $Re_D > 5,300$, the extent of the separated flow area was increased with growth of the Reynolds number. At $Re_D = 6,800$ a weak flow rotation occurred inside the dimple with a small flow fluctuations zone near the backside dimple rim. This might be due to the flow instability inside a dimple. After $Re_D = 9,200$ the in-dimple separation zone is almost symmetrical. Moreover, due to the laminar-turbulent flow transition after the first row (S2 - and S3 – streamlines at Re_D >12,250) the separation zone extent remains approximately constant at around 50% of the dimple area up to $Re_D = 23,450$. Unlike this, for the single array of dimples the separation zone extent increased monotonically with the Reynolds number growth [5, 6]. Downstream of the dimple the flow exhibits a «strip» pattern at $Re_D \leq 4,200$, while at $Re_D = 5,300$ the flow transitioned to the turbulent flow. The highly-developed downstream bulk flow fluctuations were observed at $Re_D > 5,300$.
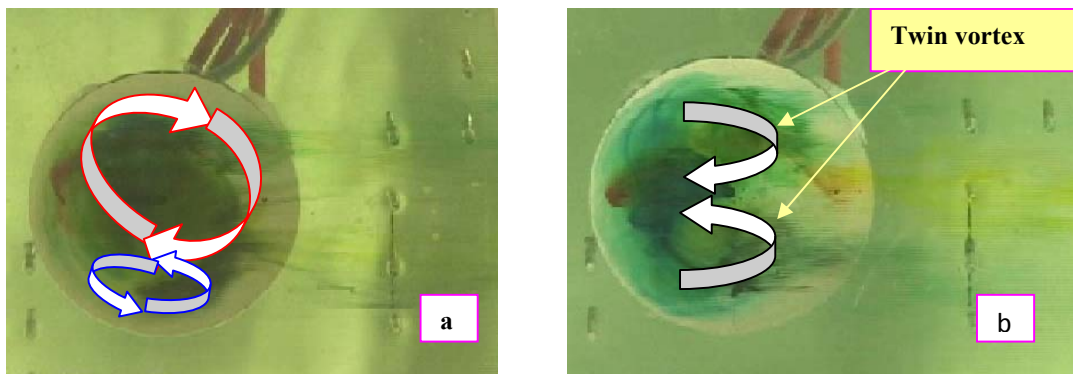
Figure 12. Flow patterns inside the spherical dimple in the second array. **a:** $Re_D = 9,500$. **b:** $Re_D = 12,250$.
Dye injection inside the dimple.

Spherical dimples. The experimental program was performed across the same range of fluid boundary conditions as for the dual array of cylindrical dimples. At low flow velocities ($Re_D=3,300$) the S1- streamline over a dimple was parallel to the axial flow direction, while S2- and S3-streamlines demonstrated the weak span-wise fluctuations. At $Re_D > 10,500$, the streamlines over the

dimple experienced substantial span-wise fluctuations. It was especially noticeable in the dimple axis area. At higher flow velocities (Re_D>12,250) the streamlines were twisted and broken.

Inside a dimple the unsteady flow pattern appeared at Re_D=5,500 with periodic downstream bulk flow fluctuations. At higher flow velocities, these fluctuations increased, so the bulk flow fluctuations become almost regular at Re_D= 8,000. At Re_D = 9,500 the asymmetric twin vortex action began inside the dimple (Fig. 12.a), which transformed into a symmetrical twin vortex pair at Re_D = 12,250 occupying around 50% of the dimple area (Fig. 12.b). At Re_D = 17,000 the twin vortex pair started to dissipate into the chaotic streamline patterns. This chaotic structure increased with increases in the flow velocity leading to fully chaotic flow in upstream dimple area. At Re_D = 23,450 the in-dimple separation zone extent reached around 70%. Downstream of a dimple, the streamlines fluctuated in the span-wise direction; increasing the flow velocity led to the growth of span-wise fluctuations and transition to the turbulent flow.

a.

b.
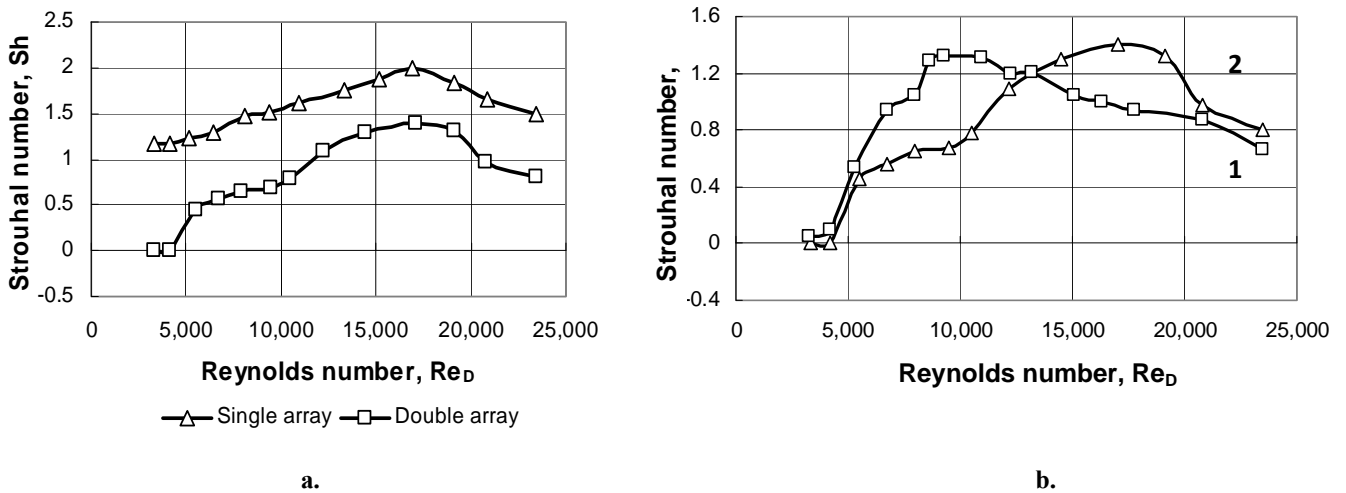
Figure 13. a: Bulk flow fluctuations downstream of the spherical dimples. **b:** Bulk flow fluctuations downstream of the dual array of dimples. 1 – cylindrical dimples. 2 – spherical dimples.

A comparison of the bulk flow fluctuation frequencies generated by the spherical dimples beyond the single- and dual array of dimples is presented in Fig. 13.a For both configurations, the magnitude of Strouhal number maximum is found at approximately the same Reynolds number however the single array generates the higher Strouhal number magnitude. for the spherical dimple this maximum occurs at a greater Reynolds number. At Re_D < 7,500 and Re_D > 12,500 the spherical dimple generates more significant bulk flow fluctuations. At Re_D numbers ranging from 5,000 to 13,000 , the fluctuation frequencies of the cylindrical dimples exceeded those for spherical dimples (Fig. 13.b). However, at Re_D > 20,000 there was no effect of the dimple shape on the magnitude of the Strouhal number. For both configurations, the maximum value of Strouhal number is approximately the same to be reached at different Reynolds numbers.

LAMINAR-TURBULENT FLOW TRANSITION

Flow visualizations carried out in this study have enabled to determine the critical Reynolds numbers ($Re_{Dcr.}$) of the laminar-turbulent flow transition beyond single dimple, single and dual array of dimples. They are as follows [6]:

Cylindrical dimples: (i) Single dimple (x/D=1.23) – = 6580; (ii) Single dimple (x/D=4.70) – = 12250; (iii) Single array of dimples – = 6670; (iv) Dual array of dimples – = 6000.

Spherical dimples: (i) Single dimple (x/D=1.23) – = 8000; (ii) Single array of dimples – = 8000; (iii) Dual array of dimples – = 9500.

NOMENCLATURE

D   dimple surface diameter, m

f   frequency of bulk flow oscillations, s^{-1}

h   dimple depth, m

L   in-dimple separation zone depth (centerline), m

Re_D Reynolds number based on dimple diameter, m

S   dimple spanwise spacing, m

Sh   Strouhal number, $f{\cdot}D\,/\,U_\infty$

U_∞ average freestream velocity, m/s

x   axial distance from the plate leading edge, m

δ boundary layer thickness, m

00   data in front of a dimple

C-streamline: along the dimple centerline.

S1-streamline: offset from the center by 0.25·D

S2-streamline: 0.5·D offset from the center

REFERENCES

1. *Bearman, P.W., & Harvey, J.K.,* Golf ball aerodynamics // Aeronautical Quarterly, pt. 2, 1976, **27**.pp. 112-122.

2. *Kiknadze, G.I., Krasnov, Yu.K., Podymako, V.F., & Khabensky,V.B.,* Self-organization of vortex structures in a water flow inside hemispherical dimples // Reports of the Russian Academy of Sciences, 1986, **291**.pp.17-20.

3. *Khalatov A.A., Byerley A., Seong-Ki Min, Ochoa D.* Flow characteristics within and downstream of spherical and cylindrical dimple on a flat plate at low Reynolds numbers // ASME Paper No GT2004-53656. 2004.

4. *Coleman H., Steele G..* Experimentation and uncertainty analysis for engineers. -John Wiley & Sons. New York, NY. 2d Edition. -1999. -275p.

5. *Khalatov A.A. & Byerley A.* Flow characteristics within and downstream of a double-row array of shallow spherical and cylindrical dimples // ASME Paper No GT2006-90403. 2006.

6. *Khalatov A.A., Borisov I.I., & Shevtsov S.V.* Heat and mass transfer and thermal-hydraulic performance of vortex and swirling flows. –The National Academy of Sciences of Ukraine. Kiev.-2005.-500c.